LBL-32539
UC-335
Preprint

Lawrence Berkeley Laboratory
UNIVERSITY OF CALIFORNIA

Materials Sciences Division

Submitted to Journal of the Electrochemical Society

Current and Potential Distributions on a Cylinder Electrode

A.J. Grabowski and J. Newman

June 1992

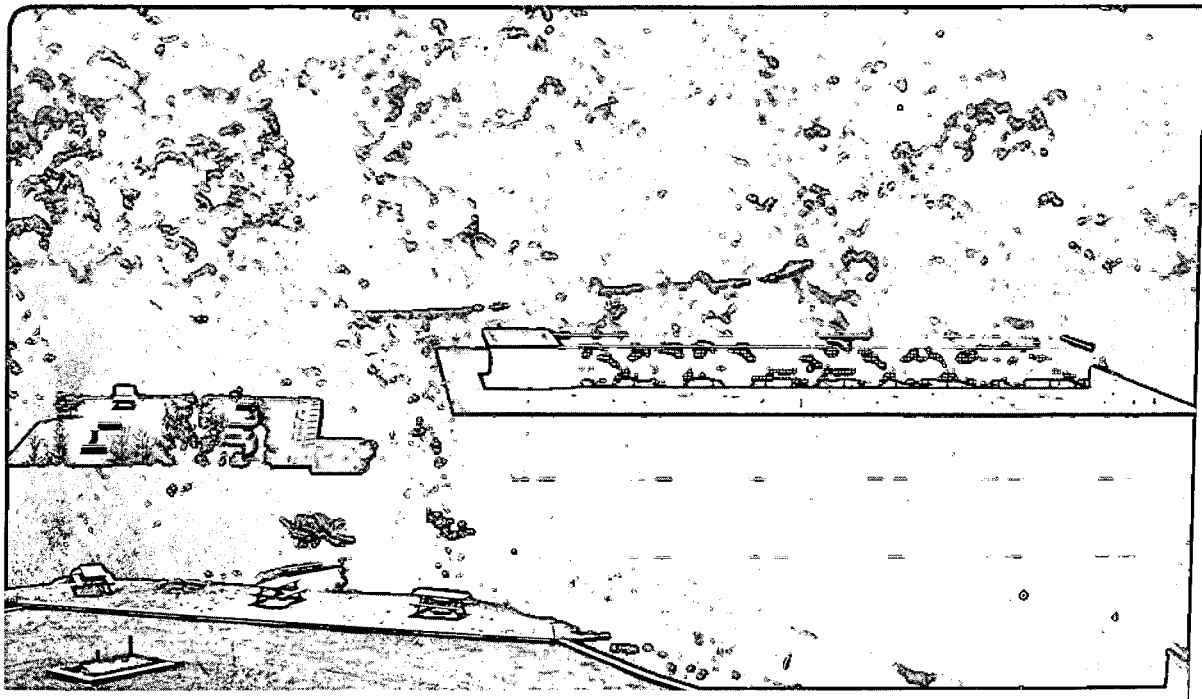

REFERENCE COPY
Does Not
Circulate
Bldg. 50 Library.
LBL-32539
Copy 1

Prepared for the U.S. Department of Energy under Contract Number DE-AC03-76SF00098

DISCLAIMER

This document was prepared as an account of work sponsored by the United States Government. While this document is believed to contain correct information, neither the United States Government nor any agency thereof, nor the Regents of the University of California, nor any of their employees, makes any warranty, express or implied, or assumes any legal responsibility for the accuracy, completeness, or usefulness of any information, apparatus, product, or process disclosed, or represents that its use would not infringe privately owned rights. Reference herein to any specific commercial product, process, or service by its trade name, trademark, manufacturer, or otherwise, does not necessarily constitute or imply its endorsement, recommendation, or favoring by the United States Government or any agency thereof, or the Regents of the University of California. The views and opinions of authors expressed herein do not necessarily state or reflect those of the United States Government or any agency thereof or the Regents of the University of California.

LBL-32539
UC-335

Current and Potential Distributions on a Cylinder Electrode

Anthony J. Grabowski and John Newman

Materials Science Division
Lawrence Berkeley Laboratory
University of California
Berkeley, California 94720

June 29, 1992

This work was supported by the Assistant Secretary for Conservation and Renewable Energy, Office of Transportation Technologies, Electric and Hybrid Propulsion Division of the U.S. Department of Energy under Contract No. DE-AC03-76SF00098.

Current and Potential Distributions on a Cylinder Electrode

Anthony J. Grabowski and John Newman

Materials Sciences Division,
Lawrence Berkeley Laboratory, and
Department of Chemical Engineering,
University of California, Berkeley

June 29, 1992

Abstract

Current and potential distributions, satisfying Laplace's equation and obtained by superposition of ring sources, are developed and discussed for a cylinder electrode embedded in an infinite insulating cylinder. For the primary distribution, the resistance and the coefficient describing how the current density goes to infinity at the edge of the electrode are presented as functions of the aspect ratio of the electrode. For a uniform current density on the electrode, the maximum potential variation on the electrode is presented as a function of the aspect ratio. For linear electrode kinetics, the condition for nearly uniform electrode current density is quantified, and the ratio of edge to center current densities is developed for kinetic parameters which lead toward the primary distribution. Current and potential distributions on the electrode and the adjoining insulator are presented for these three cases, and some asymptotic formulas are developed for high and low aspect ratios. These results are of particular interest in applications of cathodic protection.

Introduction

This work presents numerical and limiting-case solutions for the current and potential distributions of a cylinder electrode governed by Laplace's equation. Figure 1 illustrates the idealized electrochemical cell geometry and its geometric parameters: the working electrode of length $2l_0$ and radius r_0 embedded in an infinite insulating cylinder, while the counterelectrode is placed at infinity. Various electrode boundary conditions are employed, yielding the primary current distribution, the potential distribution due to uniform current density on the working electrode, and the secondary current distribution with linear kinetics.

Laplace's equation describes the potential variation in electrolytic solutions with negligible concentration gradients:

$$\nabla^2\Phi = 0. \tag{1}$$

Ohm's law gives the current density under these conditions:

$$\mathbf{i} = -\kappa\nabla\Phi. \tag{2}$$

Equations 1 and 2 govern behavior in electrochemical systems with negligible mass-transfer resistance. In particular, they apply to the bulk solution for electrochemical systems in which convection dominates mass transport and concentration gradients are confined to a thin boundary layer near the electrode surface.

The primary current distribution is characterized by negligible electrode kinetic resistance, implying negligible surface overpotential. The potential V of the working electrode is the same as the potential Φ_0 in the solution adjacent to the working electrode as measured by a reference electrode identical to the working electrode:

$$\Phi_0 = V. \tag{3}$$

With no ohmic resistance in the electrode, V is a constant, and the distribution is characterized solely by geometric parameter ratios.[1]

The primary current distribution gives maximum nonuniformity of current density. Near an electrode-insulator edge, the current density is zero at the edge for acute angles, a

Fig. 1: Electrode Geometry

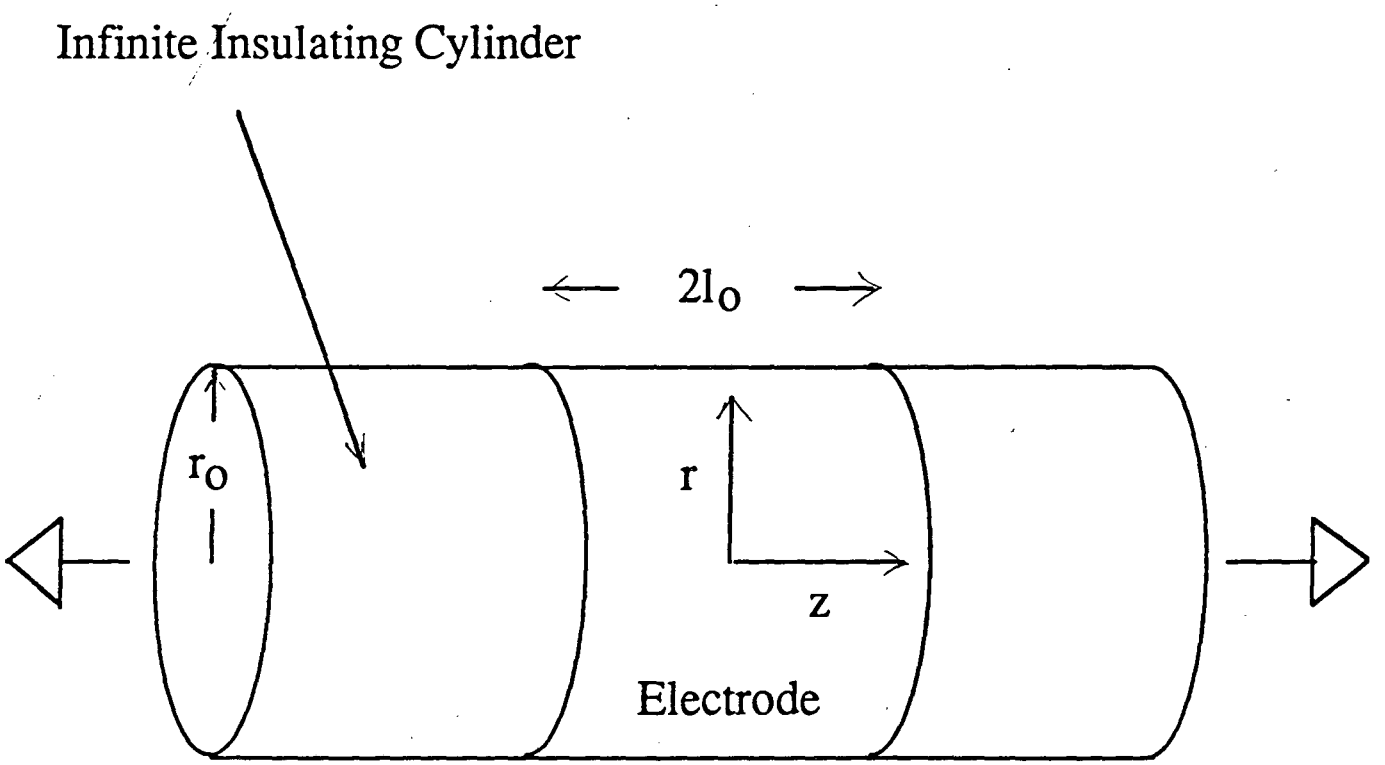

constant for right angles, and approaches infinity for obtuse angles. For the present case where the electrode is flush with the adjacent insulating surface, the primary current distribution near the edge is given by

$$i_n \rightarrow P_0 / \sqrt{x} \text{ as } x \rightarrow 0, \tag{4}$$

where i_n is the current density at the electrode, x is the distance from the electrode-insulator edge, and P_0 is a function of the system geometry.

The potential distribution due to a uniform electrode current density, governed by the same geometric parameters as the primary current distribution, provides an estimate of the maximum possible potential variation on an electrode. These constant-current-density calculations are relevant to cathodic-protection technology, where oxygen mass transport may determine the distribution of demand of current, which is provided by sacrificial anodes to protect metal objects from corroding. In these systems, the largest potential difference on the protected metal object, $\Delta\Phi_0$, must be kept within a finite range to avoid both corrosion and hydrogen evolution. This restriction dictates the maximum size of an object which a counterelectrode can protect.

The secondary current distribution, governed by Laplace's equation in solution and finite electrode kinetics, depends not only upon geometric parameter ratios but also upon the absolute size of the system. The Butler-Volmer equation is often used to describe finite electrode kinetics. In this case, the secondary current distribution depends upon three parameters in addition to the geometric parameters of the primary distribution.[1] Due to the large number of parameters, this system is difficult to analyze. The linearized Butler-Volmer equation, valid for small surface overpotentials, simplifies the problem:

$$i_n = (\alpha_a + \alpha_c)\frac{i_0 F}{RT}(V - \Phi_0) \quad \text{as} \quad \Phi_0 \rightarrow V. \tag{5}$$

In this equation i_0 is the exchange current density, α_a and α_c are the apparent transfer coefficients, F is Faraday's constant, and R is the universal gas constant. This approximation introduces an additional polarization parameter, J_r, to the governing geometric parameter ratios:

$$J_r = (\alpha_a + \alpha_c)\frac{i_0 F r_0}{\kappa RT}. \tag{6}$$

J_r represents the ratio of ohmic resistance to kinetic resistance and is the inverse of the Wagner number. As J_r approaches zero, kinetic resistance predominates, rendering the current distribution uniform on the electrode. Conversely, as J_r approaches infinity, ohmic resistance predominates, and the current distribution approaches the primary current distribution.

Most nontrivial, analytic solutions for the current distribution on finite cylindrical electrodes have been obtained for concentric electrodes with symmetric insulators at right angles to the axis of symmetry. Weisselberg[2] obtained the primary current distribution analytically in this geometry for an inner electrode with finite ohmic resistance. Waber[3] followed with an analytic solution for the secondary current distribution with linearized kinetics. Finally, Alkire and Varjian[4] solved the problem numerically, with full Butler-Volmer kinetics, for a thin resistive-wire inner electrode.

More closely related to the geometry under consideration, Strommen and Rodland[5] developed a finite-difference method for calculating potential distributions on underwater pipelines protected by exterior sacrificial anodes.

Mathematical Method

To develop an expression for the potential in the solution due to a prescribed current distribution on the electrode, we start with a differential ring located at $r = r_0$ and $z = z'$. The potential due to such a source is[6]

$$G(R^*, Z) = \frac{2K(m)}{\sqrt{Z^2 + (R^* + 1)^2}}, \tag{9}$$

where $R^* = r / r_0$, $Z = (z - z') / r_0$, and

$$m = \frac{4 r r_0}{(z - z')^2 + (r + r_0)^2}. \tag{8}$$

$K(m)$ is the complete elliptic integral of the first kind.[7] To this it is necessary to add[8] a Fourier-transform function to ensure a zero normal component of the current density on the surface of the insulating cylinder away from the ring source:

$$G^*(R^*,Z) = G + F, \tag{13}$$

where

$$F(R^*,Z) = \int_0^\infty B(\zeta) K_0(\zeta R^*) \cos(\zeta Z) d\zeta. \tag{14}$$

Here K_0 is the modified Bessel function of the second kind of order 0. The coefficient $B(\zeta)$ is obtained from the condition of zero normal derivative of G^* at $r = r_0$ and $z \neq z'$. Finally, one uses a superposition integral to represent the potential due to a distribution of ring sources along the electrode:

$$\Phi(r,z) = \frac{1}{\pi\kappa} \int_{-l_0}^{l_0} G^*(R^*,Z) i_n(z') dz'. \tag{17}$$

The idea then is to adjust $i_n(z')$ so as to satisfy certain specific boundary conditions on the surface of the electrode. In particular, equation 3 applies for the primary current and potential distribution, equation 5 applies for the secondary distribution, and $i_n = i_c$, a constant, for the case of a uniform current density on the electrode. The other boundary conditions, at infinity where the potential approaches zero and on the insulating portion of the cylindrical surface, are automatically satisfied by equation 17, which also satisfies Laplace's equation 1 by the method of construction.

Since we are most interested in conditions on the electrode surface, both to satisfy the boundary conditions and to understand the electrode processes, we focus on the value of G^* and of F on the cylindrical surface at $r = r_0$. Mak[8] carried out integrations to obtain first $B(\zeta)$ and then $F(1,Z)$. An approximate expression of these results is

$$F(1,Z) = \frac{-\pi/2}{\sqrt{Z^2+1}}. \tag{18}$$

More precise fitting functions can be found elsewhere.[9] On the cylinder, $G^*(1,Z)$ behaves in three fairly distinct fashions depending on distance from the ring source. For small Z, m approaches one, and K approaches infinity logarithmically. In this region, the ring source appears as a line source embedded in an infinite insulating plane, and G* behaves accordingly:

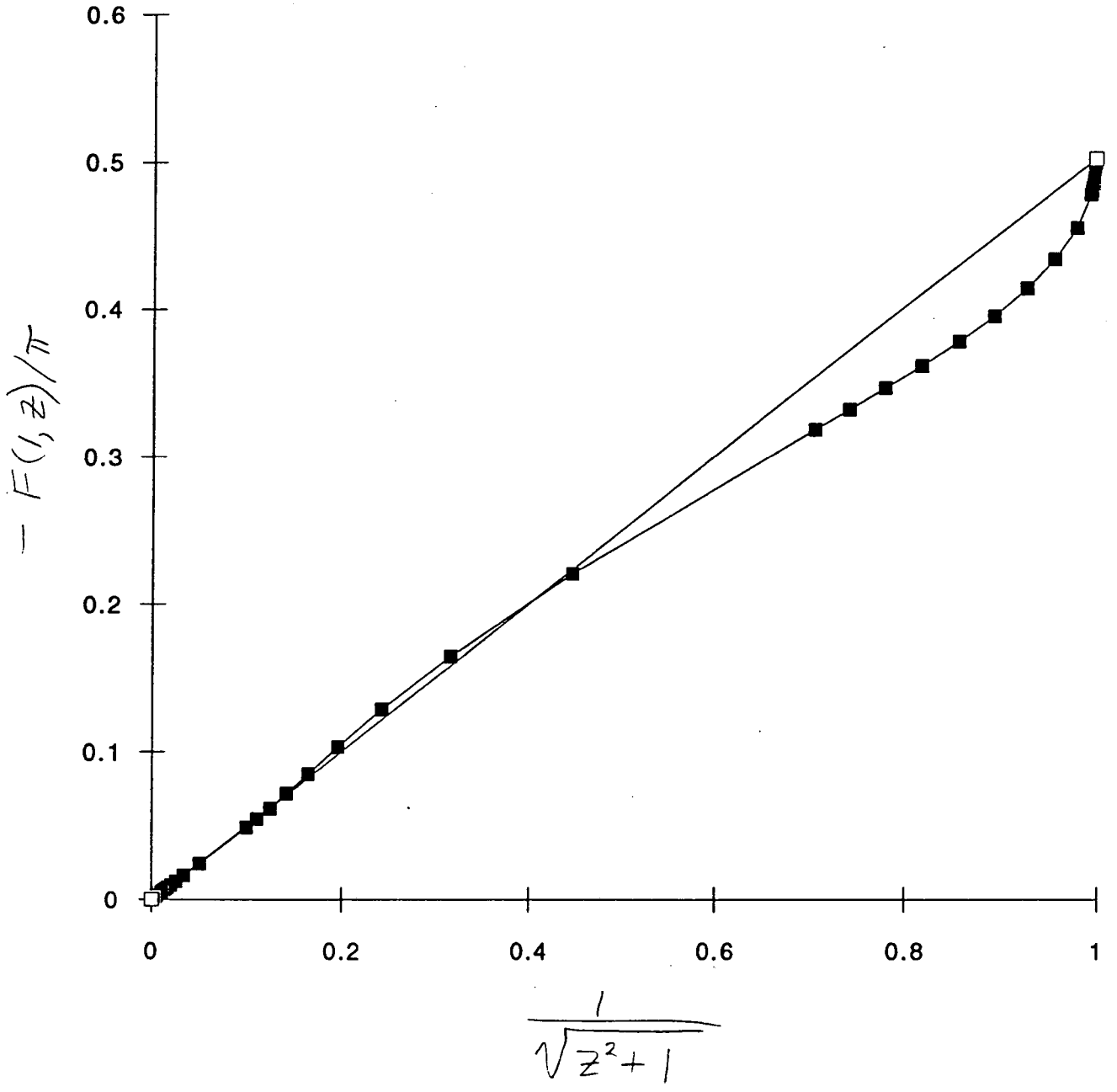
0.6
0.5
0.4
0.3
0.2
0.1
0
$-F(1,z)/\pi$
0
0.2
0.4
0.6
0.8
1
$\frac{1}{\sqrt{z^2+1}}$

$$G^*(1,Z) \to -\frac{\pi}{2} + \frac{1}{2}\ln(64/Z^2) \quad \text{as} \quad Z \to 0. \tag{15}$$

For distances of $O(r_0)$, the ring appears as a three-dimensional object and requires the full form of equation 13 to describe the potential variation. Finally, as Z approaches infinity, $K(m)$ approaches $\pi/2$, and the ring behaves as a point source. Equation 13 becomes:

$$G^*(1,Z) \to \frac{\pi}{2|Z|} \quad \text{as} \quad |Z| \to \infty. \tag{16}$$

For the primary and secondary current distributions, the electrode current density can be represented as a linear combination of functions $f_j(z')$:

$$i_n(z') = \sum_j a_j f_j(z'), \tag{24}$$

where the a_j's are adjustable constants. The first function is chosen to approximate the expected current-distribution behavior. For example, for the primary current distribution, it would be chosen to go to infinity at the electrode edges like equation 4. The rest of the current functions were chosen to be the first 20 even Legendre polynomials:

$$i_n(z') = a_{-1} f_{-1}(z') + \sum_{j=0}^{19} a_j P_{2j}(z'/l_0). \tag{28}$$

In general, the secondary-current fitting functions do not use a special first fitting function. However, for high polarization parameters, the work of Nişancioğlu and Newman[10] and Smyrl and Newman[11] is used to develop a tailored first fitting function which approaches the actual secondary current distribution in the small electrode-edge region where kinetic limitations are important and the primary current distribution away from the edge region where kinetic limitations are negligible.

To solve for the a_j's in equation 24, a collocation technique is employed. For n current functions, the boundary condition is evaluated at n points on the electrode, generating an $n \times n$ matrix. Using the zeros of the Legendre polynomials and the electrode edge as collocation points provided the best results. Integrations were carried out using Simpson's rule.

Results were considered accurate when the boundary conditions were satisfied to within 0.01% at each sampled electrode boundary point. In addition, primary current distributions, using different first functions valid for large and small l_0 / r_0 respectively, were compared for l_0 / r_0=10 and l_0 / r_0=100. For both aspect ratios, the difference between the results for the two functions was within 0.1% . Secondary-current-distribution results, also using different first functions valid for large and small l_0 / r_0, were compared for l_0 / r_0 =1 and J_r=10 . These results also differed by less than 0.1%.

Results and Discussion

Both the primary current distribution and the potential distribution due to constant current density on the electrode were calculated for values of l_0 / r_0 from 0 to 1000. Beyond this range, the method broke down because the Legendre-polynomial correction functions were unable to satisfy the boundary condition in the edge region of $O(r_0)$ where the distributions vary greatly as l_0 / r_0 becomes large.

The secondary current distribution could be calculated accurately for aspect ratios between zero and ten for the entire polarization-parameter range. Beyond l_0 / r_0=10, results could be obtained only for large and small J_r.

Primary current distribution.--Ohmic resistance in solution determines the primary current distribution, which then becomes a unique function of cell geometry.[1] In the present case, the only geometric parameter is the ratio l_0 / r_0 . Figure 2 shows the primary current distribution. For all l_0 / r_0, the electrode current density approaches infinity inversely proportional to the square root of distance from the electrode-insulator edge, as described by equation 4.

In the limit of small l_0 / r_0, the cylinder loses its curvature, appearing as an infinite strip embedded in an infinite plane. The primary distribution for an infinite strip has been given by Wagner[12]

$$\frac{i_n}{i_{avg}} = \frac{2/\pi}{\sqrt{1-(z/l_0)^2}}. \tag{31}$$

Fig. 2: Primary Current Distribution

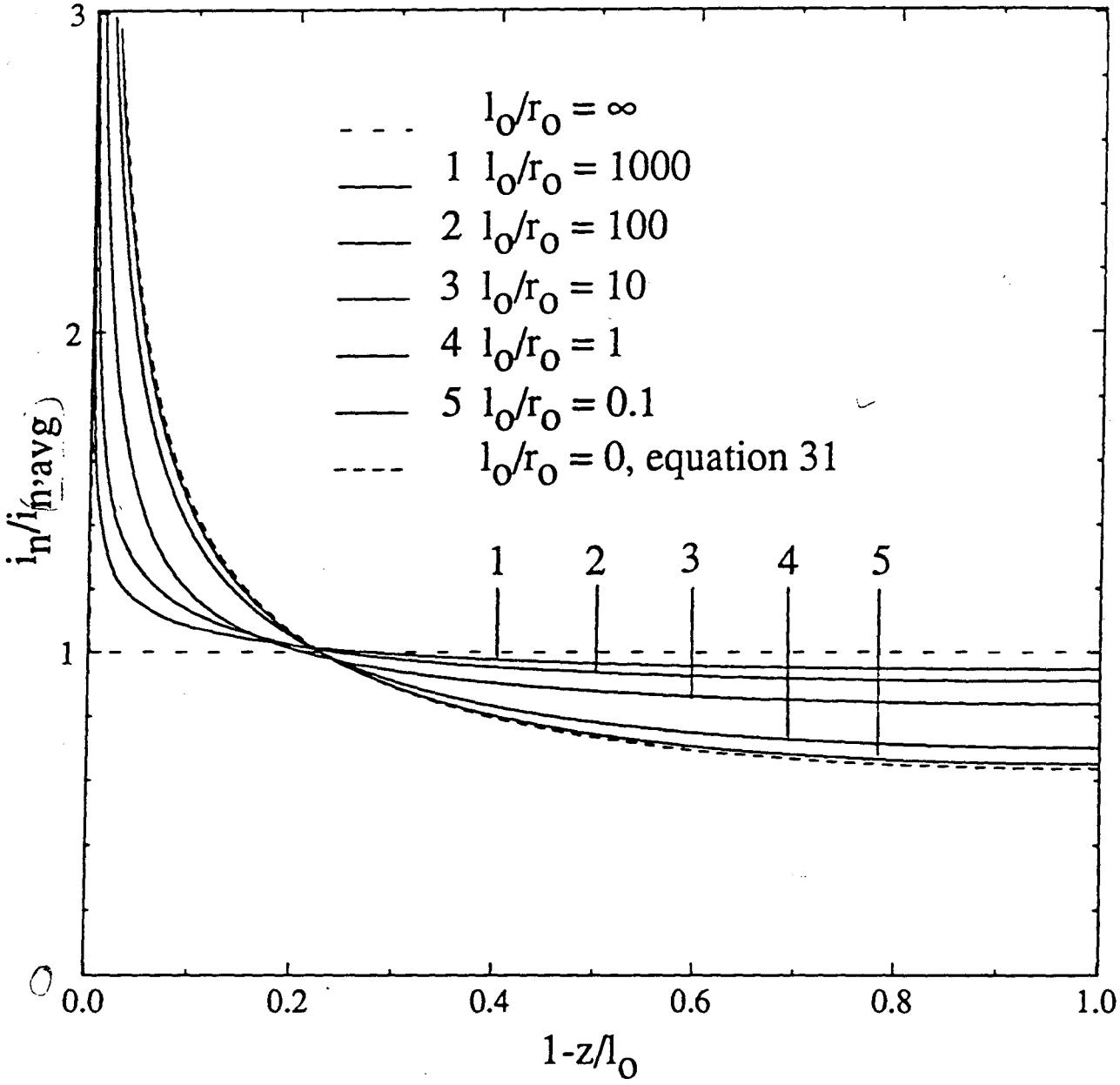

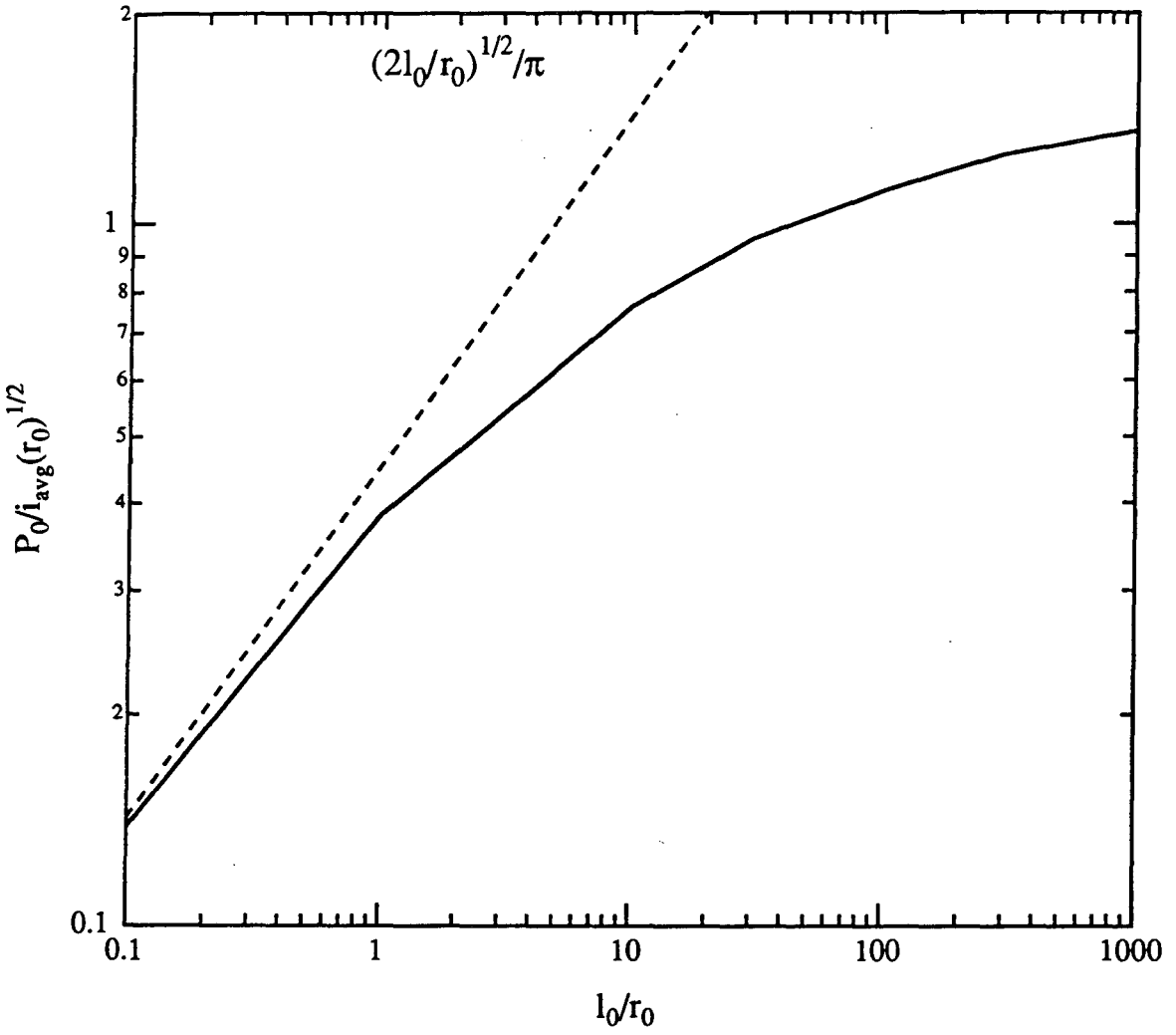

Figure 3. Asymptotic coefficient for the primary current near the electrode edge.

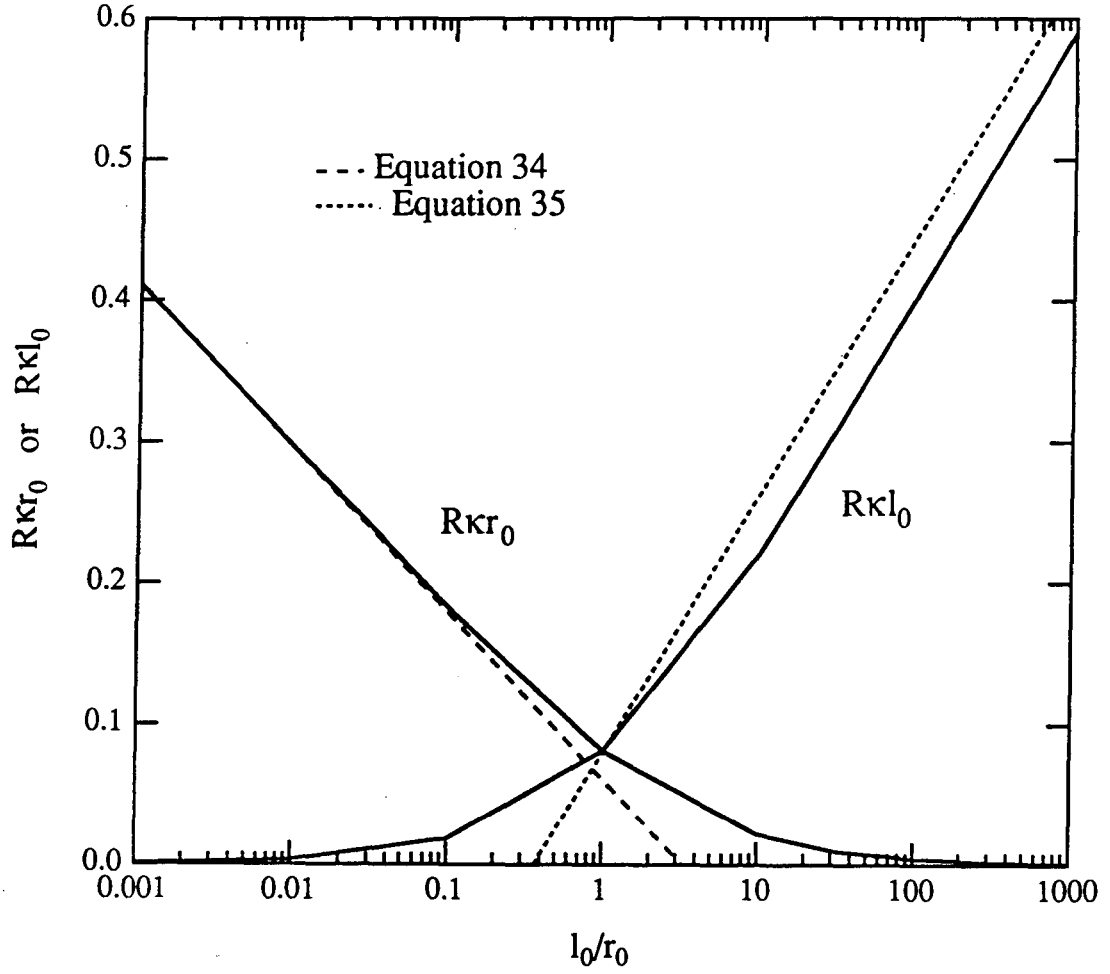

Figure 4. Ohmic resistance.

/In the opposite extreme, as l_0 / r_0 becomes large, the electrode current density approaches infinity in an edge region which grows increasingly smaller when compared with l_0. Then the mid region carries all the current, and the singularity at the edge appears as a spike of current. The current distributions for finite l_0 / r_0 fall between these two cases.

To understand further the singular behavior in the edge region, one can examine the asymptotic coefficient of equation 4. Figure 3 shows $P_0 / i_{avg}\sqrt{r_0}$ as a function of l_0 / r_0, along with the thin-strip asymptote embodied in equation 31. The asymptotic behavior at large aspect ratios, where the electrode appears as a semi-infinite cylinder when viewed from one end, could not be determined.

The primary resistance describes the relationship between the potential difference and total current in a cell limited by ohmic resistance. It is convenient to use two dimensionless resistances for the cylinder-electrode system, $R\kappa r_0$ and $R\kappa l_0$, related by l_0 / r_0. As l_0 / r_0 approaches zero and the cylinder electrode shrinks to a differentially thin ring, $R\kappa r_0$ approaches infinity. At the other extreme, as l_0 / r_0 approaches infinity and the cylinder shrinks to a differentially thin needle, $R\kappa l_0$ approaches infinity. Figure 4 is a graph of the dimensionless resistances as functions of l_0 / r_0.

Using asymptotic expressions for $K(m)$, i_n, and $F(1,Z)$ valid for thin rings, one finds that $R\kappa r_0$ approaches infinity logarithmically as the aspect ratio shrinks according to the following expression:

$$R\kappa r_0 \rightarrow \frac{-1}{4\pi} + \frac{\ln(16 r_0 / l_0)}{2\pi^2} \quad \text{as} \quad l_0 / r_0 \rightarrow 0. \tag{34}$$

For asymptotically large l_0 / r_0, figure 2 shows that the current density is essentially constant over the electrode except for a spike of current at the edges. Thus, for resistance calculations, it is reasonable to assume constant current density on the electrode. At a distance from the electrode much greater than l_0, the electrode behaves as a point source. Setting the potential for a cylinder source and a point source equal at a distance of $O(l_0)$ results in the following approximate equation for $R\kappa l_0$:

$$4\pi R\kappa l_0 \approx 1 + \ln(l_0 / r_0) \quad \text{as} \quad l_0 / r_0 \rightarrow \infty. \tag{35}$$

Here $R\kappa l_0$ approaches infinity logarithmically as l_0 / r_0 becomes large. According to figure 4, this equation is evidently off by a small additive constant, but it gives the correct slope. A better fit is achieved if 1 on the right side of equation 35 is replaced by 0.5.

Combination of P_0 and R allows one to relate the current-density behavior at the electrode edge to the cell potential V. Table 1 presents values for the edge coefficient P_0, the primary resistance R, and the maximum potential variation $\Delta\Phi_0$ over the surface of an electrode of uniform current density (discussed in the next subsection).

Table 1. Overall results for the primary and uniform current distributions.

l_0 / r_0	$R\kappa r_0$	$P_0 / i_{avg}\sqrt{l_0}$	$\kappa\Delta\Phi_0 / i_c l_0$
0.001	0.411	0.450	0.441
0.01	0.295	0.449	0.439
0.1	0.181	0.438	0.419
1	0.0809	0.383	0.322
10	0.0220	0.240	0.118
30	0.0102	0.173	--
100	0.00403	0.111	0.0237
300	0.00164	0.0721	--
1000	0.000589	0.0421	0.00353

Potential distribution due to uniform electrode current density.--The potential distribution due to constant $i_n = i_c$ gives an estimate of the maximum possible potential variation on an electrode. In the cylinder electrode system, l_0 / r_0 alone governs this potential distribution. Figure 5 shows the potential distribution along the electrode and the insulator for small values of l_0 / r_0. Note that the primary resistance provides an initial estimate of the potential in the neighborhood of the electrode. The potential is bowed upward on the electrode to counteract the tendency for a high current density near the electrode edge (as evidenced in the primary current distribution in figure 2). The maximum potential variation from one point to another in the solution adjacent to the electrode is displayed in figure 6. We next examine the behavior for small and large aspect ratios.

Fig. 5: Potential Due to Constant i_n for Small l_o/r_o

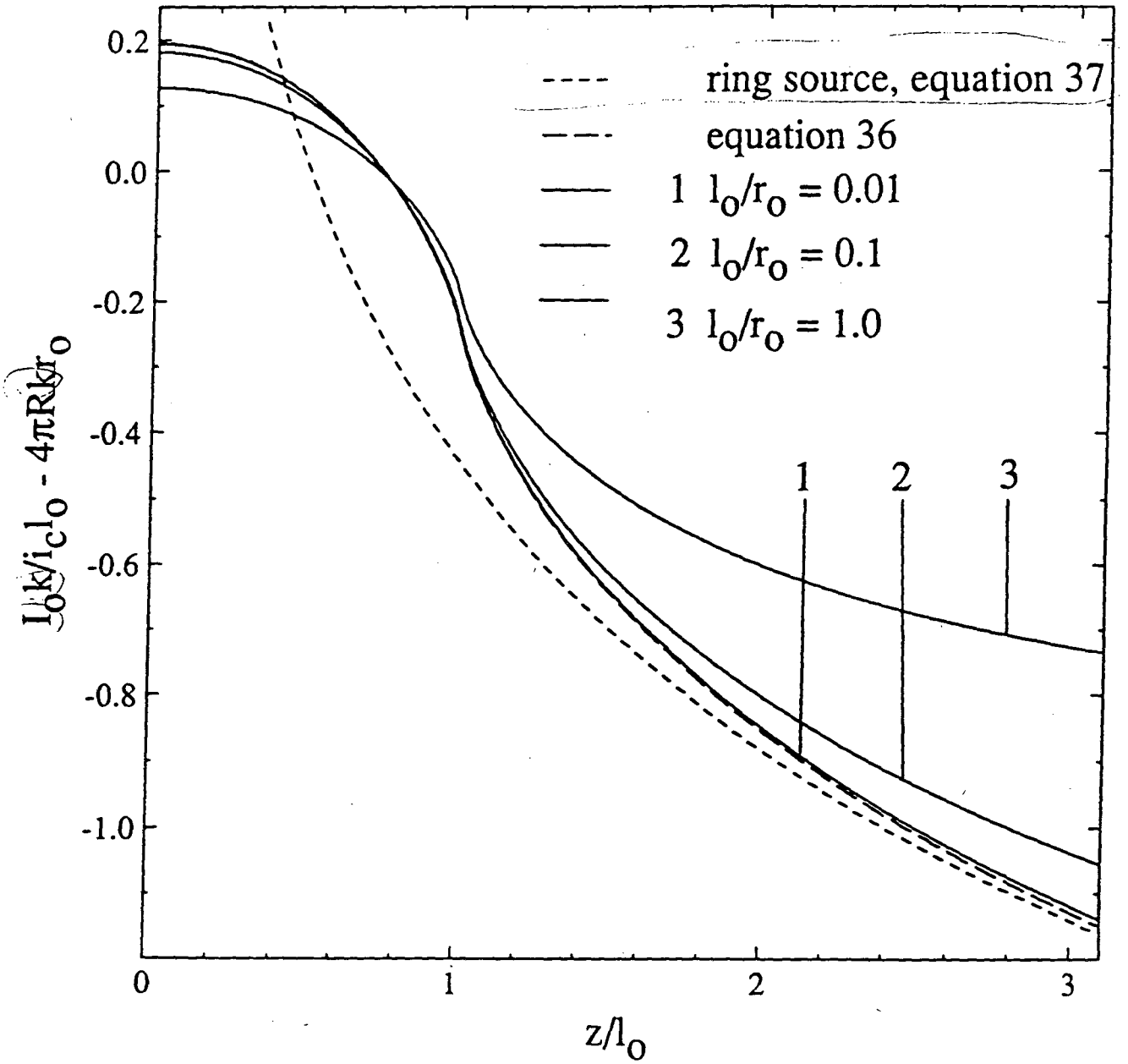

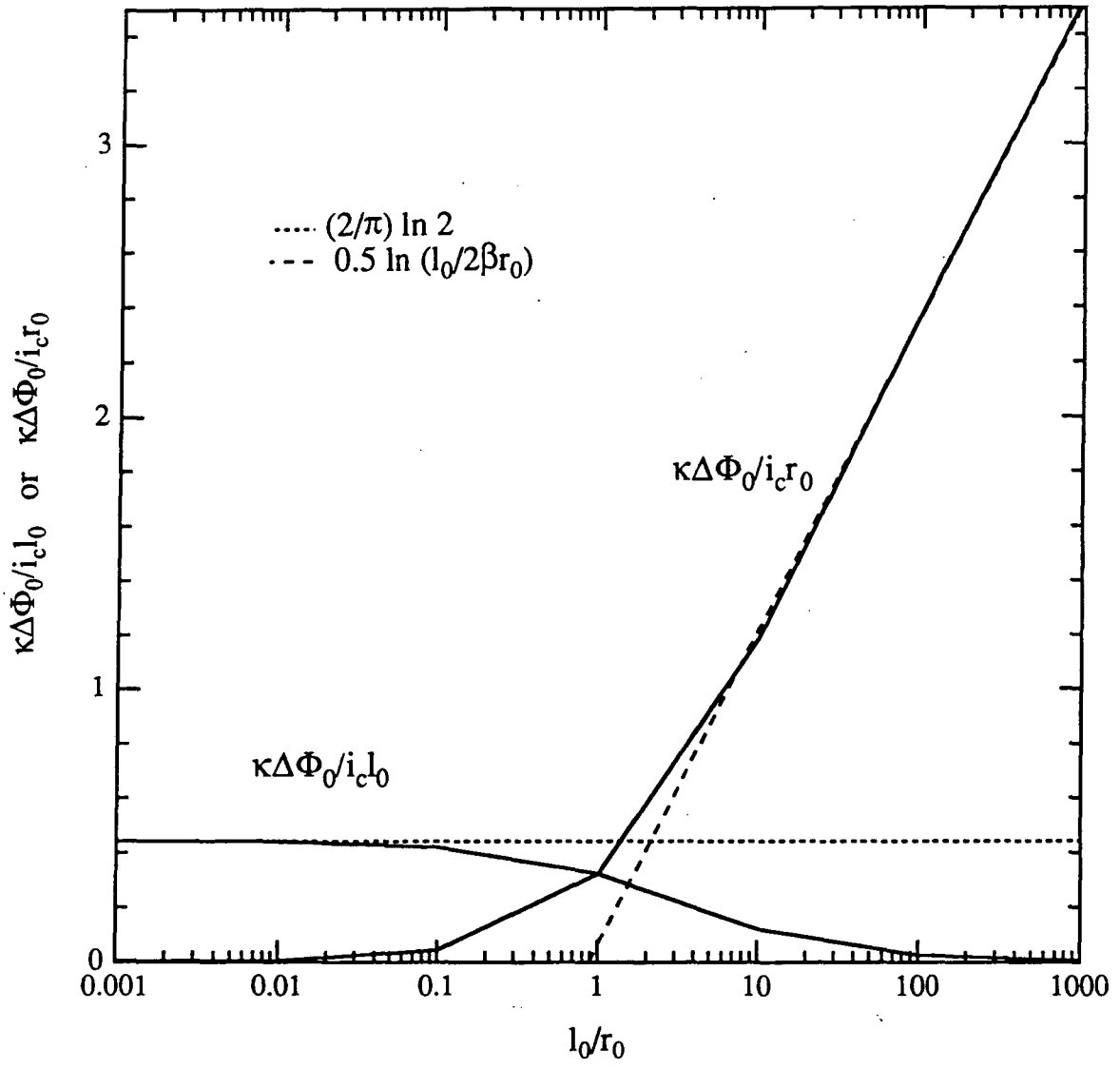

Figure 6. Maximum potential variation on the electrode with a uniform current density. (β=0.44.)

As l_0 / r_0 approaches zero, one can imagine four regions in the solution in which the potential due to constant i_n varies in distinctly different fashions. For distances of $O(l_0)$ from the electrode surface, the electrode appears to have no curvature and finite width. When one moves farther out into solution--to distances between $O(l_0)$ and $O(r_0)$--the electrode still appears to have no curvature, but now appears as a line source. Here, the potential varies logarithmically according to equation 15. When one moves still farther out, to distances of $O(r_0)$, the electrode appears as a ring source. Consequently, the full ring-source expression, equation 13, is needed to determine the potential distribution. Finally, for distances much greater than r_0, the electrode appears as a point source, and equation 16 governs the potential distribution. Such regions also exist for the primary and secondary distributions for small l_0 / r_0; only the detailed distribution in the first region, of $O(l_0)$, is different.

With similiar approximations to those used in deriving equation 34, the potential variation on the electrode and insulator for distances of $O(l_0)$ and small l_0 / r_0 can be expressed as

$$\frac{\kappa\Phi_0}{i_c l_0} - 4\pi R\kappa r_0 = \frac{1}{\pi}\left\{2 - 2\ln 2 + \left(\frac{z}{l_0} - 1\right)\ln\left|\frac{z}{l_0} - 1\right| - \left(\frac{z}{l_0} + 1\right)\ln\left|\frac{z}{l_0} + 1\right|\right\}. \tag{36}$$

This result is plotted on figure 5 and nearly coincides with the curve for l_0 / r_0=0.01. The potential difference between the center and the edge of the electrode follows from equation 36. The limit of $(2/\pi)\ln 2$ is shown on figure 6. These thin-strip limits, including equation 36, also apply to a strip electrode embedded in an infinite plane.

For large l_0 / r_0, there are six fairly distinct regions on the electrode cylinder and insulator where the potential varies in distinct fashions. From the middle of the cylinder to an edge distance much greater than r_0, one expects the potential distribution to be fairly flat, like that due to an infinitely long cylinder electrode. For distances of $O(r_0)$ from the edge, the electrode appears as a semi-infinite cylinder electrode. At edge distances much less than r_0, the edge region appears as a large planar electrode adjacent to a large

insulating plane. On the insulator, for distances from the edge much greater than r_0 but much less than l_0, the electrode appears as a semi-infinite line source. For distances from the edge of $O(l_0)$, on the insulator, the electrode appears as a finite line source. Finally, at distances much greater than l_0, the cylinder behaves as a point source. Figure 7 shows the potential distribution on the electrode for large values of l_0 / r_0. Figure 8 covers the edge region, on both the electrode and the insulator.

At large l_0 / r_0, the portion of the integrand where $z - z' >> r_0$ provides the major contribution to the integral in equation 17. To obtain an estimate for the potential on the electrode surface and insulator, one can approximate this integral as:

$$\frac{\kappa\Phi_0}{i_c r_0} \approx \frac{1}{2}\int_{-l_0}^{l_0} \frac{dz'}{\sqrt{(z-z')^2 + 4(\beta r_0)^2}}. \tag{39}$$

Here the ring-like behavior for finite $(z - z') / r_0$ is lumped into an adjustable constant β. Evaluation of the above integral yields

$$\frac{\kappa\Phi_0}{i_c r_0} \approx \frac{1}{2}\left\{\ln\left[\frac{l_0 - z}{2\beta r_0} + \sqrt{\left(\frac{l_0 - z}{2\beta r_0}\right)^2 + 1}\right] + \ln\left[\frac{l_0 + z}{2\beta r_0} + \sqrt{\left(\frac{l_0 + z}{2\beta r_0}\right)^2 + 1}\right]\right\}. \tag{40}$$

This equation, valid on both the electrode and the insulator, equals $\ln(l_0 / \beta r_0)$ at the middle of the electrode and $0.5\ln(2l_0 / \beta r_0)$ at the electrode edge and approaches l_0 / z far from the electrode. Computer-generated results for potentials at the center of the electrode were used to fit a β-value of 0.44.

On the electrode away from the edge, equation 40 reduces to:

$$\frac{\kappa\Phi_0}{i_c r_0} - \ln\left(\frac{l_0}{\beta r_0}\right) \approx \frac{1}{2}\ln\left(1 - \frac{z^2}{l_0^2}\right). \tag{41}$$

This limiting form is convenient to plot on figure 7, although it approaches minus infinity at the edge itself. [Since we treated the primary resistance R in the limit of large l_0 / r_0 by reference to the case of a uniform current density, it is appropriate to note that the potential value at the middle of the electrode corresponds to $4\pi R\kappa l_0 = \ln(l_0 / \beta r_0)$. However, integration of equation 41 to obtain an average value of the potential gives $4\pi R\kappa l_0 \approx -1$

Fig. 7: Electrode Potential for Large l_o/r_o

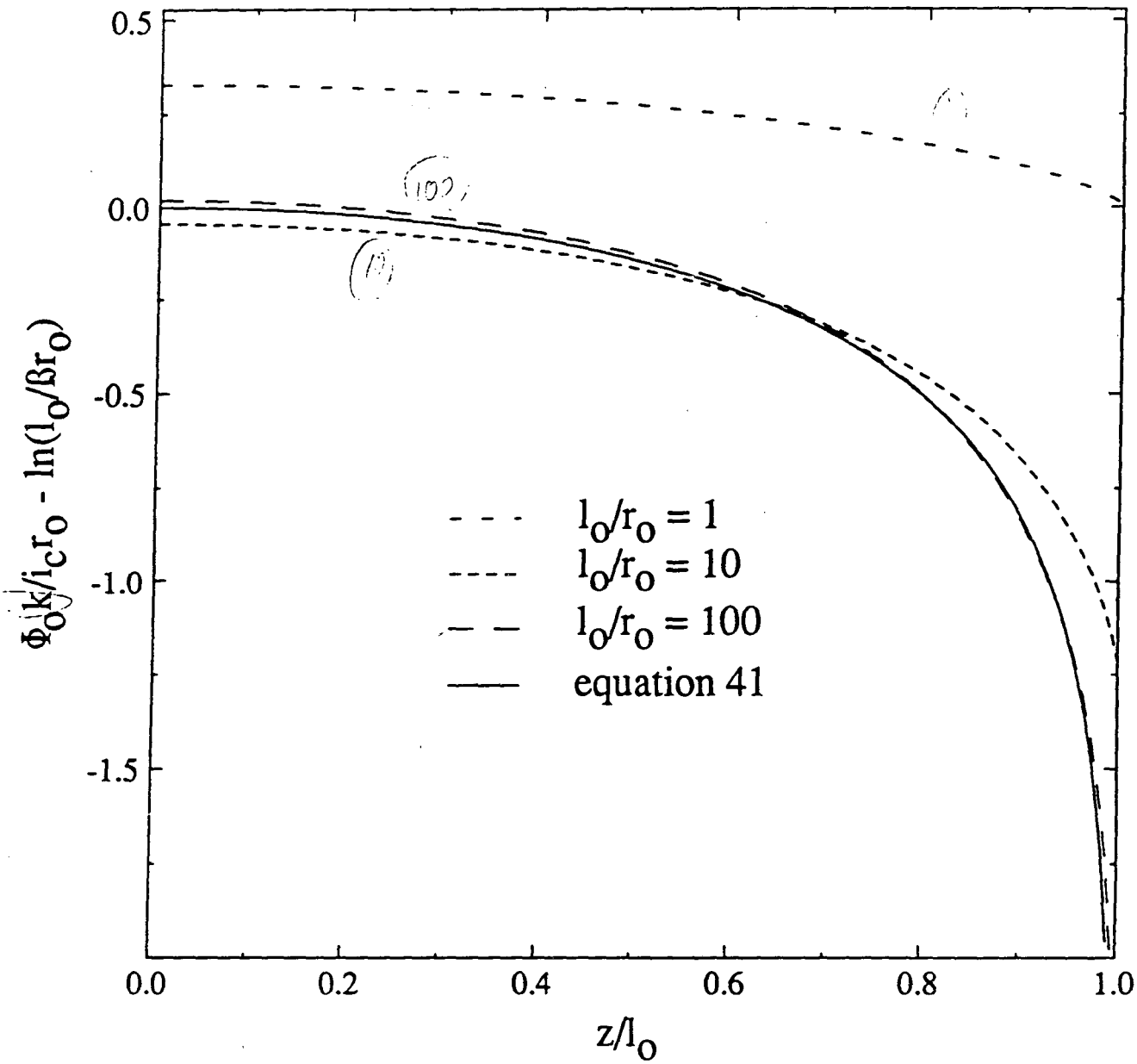

Fig 8: Potential in $O(r_o)$ edge region for large l_o/r_o

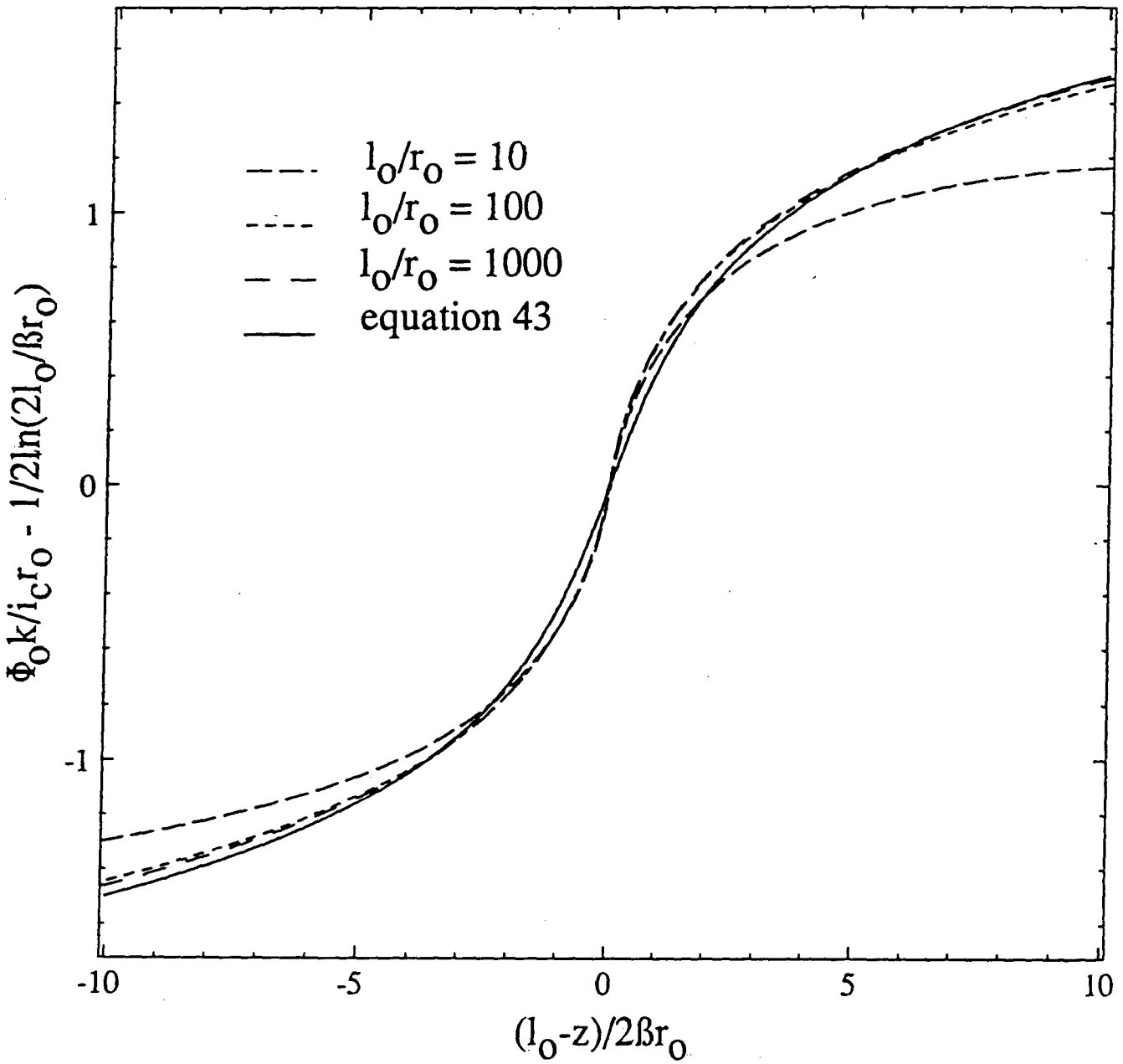

$+\ln(2l_0 / \beta r_0)$. This would permit improved agreement for the asymptote for large l_0 / r_0 in figure 4.]

The potential difference between the center and the edge of the electrode also follows from equation 40:

$$\frac{\kappa \Delta\Phi_0}{i_c r_0} \approx \frac{1}{2}\ln\left(\frac{l_0}{2\beta r_0}\right) \quad \text{for} \quad \frac{l_0}{r_0} \to \infty. \tag{48}$$

Figure 6 shows this asymptote along with numerically generated potential differences. The value of β=0.44 works well here also.

For distances from the edge of $O(r_0)$, equation 40 reduces to

$$\frac{\kappa\Phi_0}{i_c r_0} - \frac{1}{2}\ln\left(\frac{2l_0}{\beta r_0}\right) \approx \frac{1}{2}\ln\left[\frac{l_0 - z}{2\beta r_0} + \sqrt{\left(\frac{l_0 - z}{2\beta r_0}\right)^2 + 1}\right]. \tag{43}$$

This limiting form is convenient to plot on figure 8, showing the edge region. Although equation 43 reproduces the potential at the edge very well, it fails to show that the potential profile actually has an infinite slope at this point. This discrepancy occurs because the integrand in equation 39 poorly approximates the variation in the ring source $G^*(1,Z)$ for Z close to zero. This is not a problem away from the edge, on either the electrode or the insulator, or at the edge itself because β can compensate for the contribution of the small-Z region.

Correction for the approximation of the integrand for edge distances much less than r_0, *i.e.*, where the electrode-insulator region appears planar, shows that the potential on the surface takes the form

$$\frac{\kappa\Phi_0}{i_c r_0} - \frac{1}{2}\ln\left(\frac{2l_0}{\beta r_0}\right) + \frac{l_0 - z}{4l_0} + \frac{l_0 - z}{\pi r_0}\ln\left|\frac{l_0 - z}{r_0}\right| = 0.4802\frac{l_0 - z}{r_0}. \tag{45}$$

This equation is in good agreement with the numerical results for large l_0 / r_0 in the edge region and reproduces the infinite slope at the edge, but those results suggest that the coefficient on the right might be 0.5 or 0.52 instead of 0.4802.

Secondary current distribution.--The secondary current distribution takes into account finite electrode kinetics and ohmic resistance in solution. Thus, in addition to

geometric parameters which govern the primary distribution on an electrode, additional kinetic parameters determine the secondary current distribution. For small surface overpotentials, the linear-kinetics approximation can be invoked, introducing the polarization parameter J_r as a governing parameter.

The secondary current distribution on the cylinder electrode for linear kinetics is dictated by the geometric ratio l_0 / r_0 and either J_r or J_l, where J_l is a polarization parameter formed as in equation 6 but with r_0 replaced by l_0. Figure 11 illustrates the parameter space; large J_r is toward the right, large J_l is toward the top, and large l_0 / r_0 is toward the upper left. This diagram can help us visualize where certain asymptotic results apply.

Figure 12 portrays the results for the secondary current distribution for l_0 / r_0=1. Since J_r represents the ratio of ohmic resistance to kinetic resistance, the current distribution approaches the primary distribution as J_r approaches infinity and ohmic resistance predominates. Conversely, the current density becomes uniform over the entire electrode as J_r approaches zero and electrode kinetic resistance predominates. Current distributions for finite J_r fall between these two extremes.

Nişancioğlu and Newman[10] and Smyrl and Newman[11] examined how the secondary current distribution approaches the primary distribution for large polarization parameters (the upper right in figure 11). They showed that when ohmic effects dominate, the current distribution deviates from the primary current distribution only in a small edge region of order σ, where $\sigma = RT\kappa / (\alpha_a + \alpha_c)Fi_0$. In this edge region, the current distribution is relatively independent of the details of the cell's geometry. Away from this edge region, toward the center of the electrode, the current distribution approaches the primary distribution. In the cylinder-electrode problem, there are two important geometric distances. The current distribution will be relatively independent of cell geometry in the edge region only if σ is small compared to both r_0 and l_0, so that the edge region is

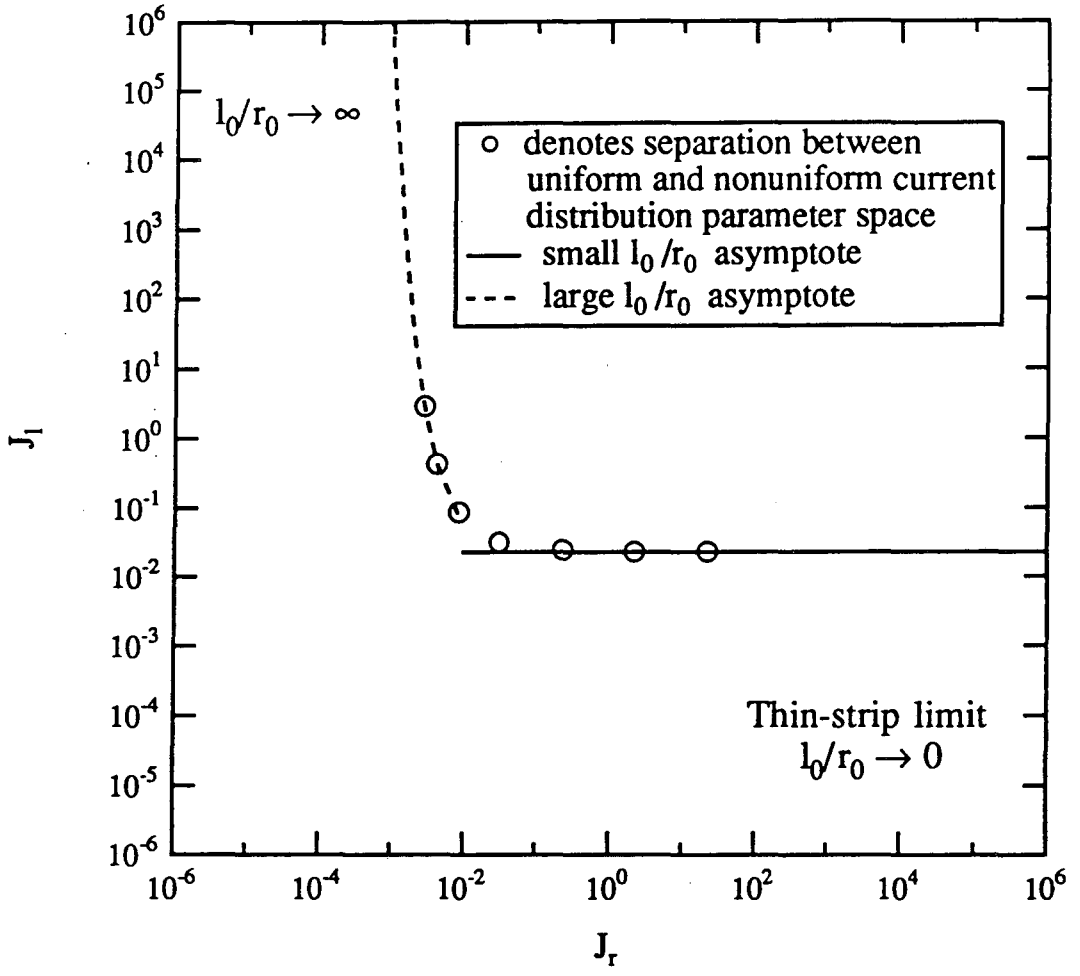

Figure 11. Parameter space for the secondary current distribution. Low aspect ratios in the lower right represent the thin-strip limit, already treated in the literature. The primary distribution is approached toward the upper right; the uniform current distribution toward the bottom and the left.

Fig. 12: Secondary Current Distribution, l_o/r_o=1.0

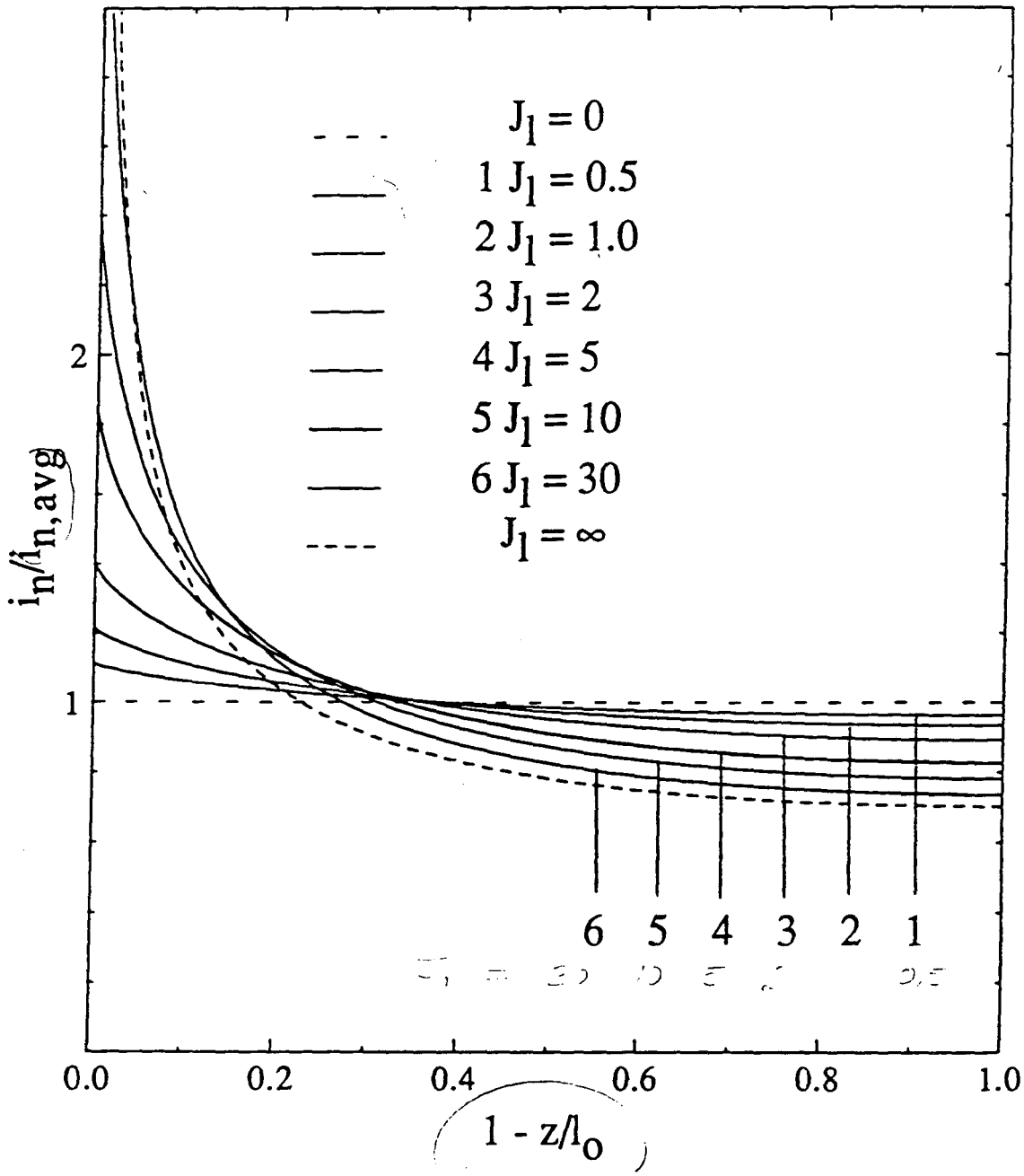

approximately planar and constitutes only a small part of the electrode. Thus, both J_r and J_l must be large.

Nişancioğlu and Newman[10] solved the edge-region problem for an electrode-insulator intersection angle of 180 degrees. In terms of the cylinder-electrode problem, the current distribution takes the form[11]

$$i_n\sqrt{\sigma}\,/\,P_0 = \phi(x\,/\,\sigma) \tag{49}$$

in the edge region, where ϕ is a universal function of the stretched edge variable $x\,/\,\sigma$. At the electrode edge, ϕ equals 1.75; as the stretched variable $x\,/\,\sigma$ approaches infinity, ϕ approaches the edge-region primary distribution given in equation 4. Figure 13 shows the secondary current distribution for $l_0\,/\,r_0$=1 plotted as suggested by equation 49 and approaching a universal function for large J_r.

Since ϕ equals 1.75 at the electrode edge, the ratio of the edge current to the average current can be written as

$$\frac{i_{\text{edge}}}{i_{\text{avg}}} \rightarrow \frac{1.75P_0}{i_{\text{avg}}\sqrt{r_0}}\sqrt{J_r} \quad \text{as} \quad J_l \rightarrow \infty \quad \text{and} \quad J_r \rightarrow \infty, \tag{51}$$

and one can apply the results from figure 3. For example, for vanishing $l_0\,/\,r_0$,

$$\frac{i_{\text{edge}}}{i_{\text{avg}}} \rightarrow \frac{1.75\sqrt{2}}{\pi}\sqrt{J_l} \quad \text{as} \quad J_l \rightarrow \infty \quad \text{and} \quad \frac{l_0}{r_0} \rightarrow 0. \tag{53}$$

As $l_0\,/\,r_0$ nears zero (the lower right in figure 11), the secondary current distribution approaches the thin-strip limit, leaving J_l as the only governing parameter. The thin-strip limit has been treated by Wagner[12] and by Parrish and Newman.[13] Figure 14 illustrates how the current distribution becomes a function of J_l alone in the limit of small $l_0\,/\,r_0$.

Finally, we can define the demarcation, sketched on figure 11, separating the region of uniform current distribution from the rest of the parameter space. With a nearly uniform current distribution, the potential difference between the solution adjacent to the center and the edge of the electrode is given by $\Delta\Phi_0$, plotted in figure 6. The linearized Butler-Volmer equation 5 then yields the ratio of current densities at the edge and center of the electrode:

Fig. 13: Secondary Current Dist. ~~for Large J_l, l_o/r_o=1.0~~

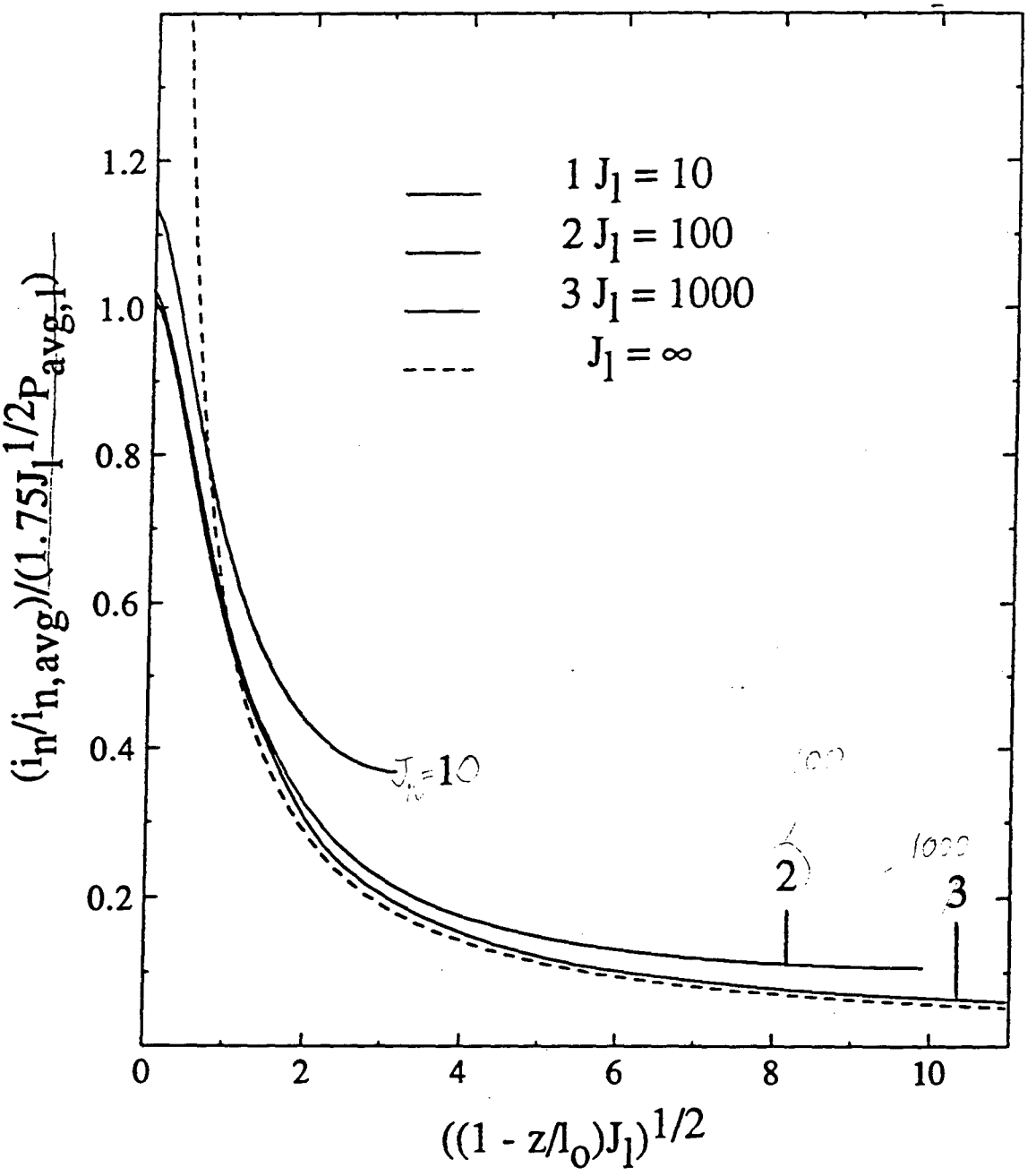

Fig. 14: Secondary Current Dist. for Small l_o/r_o, J_l=10

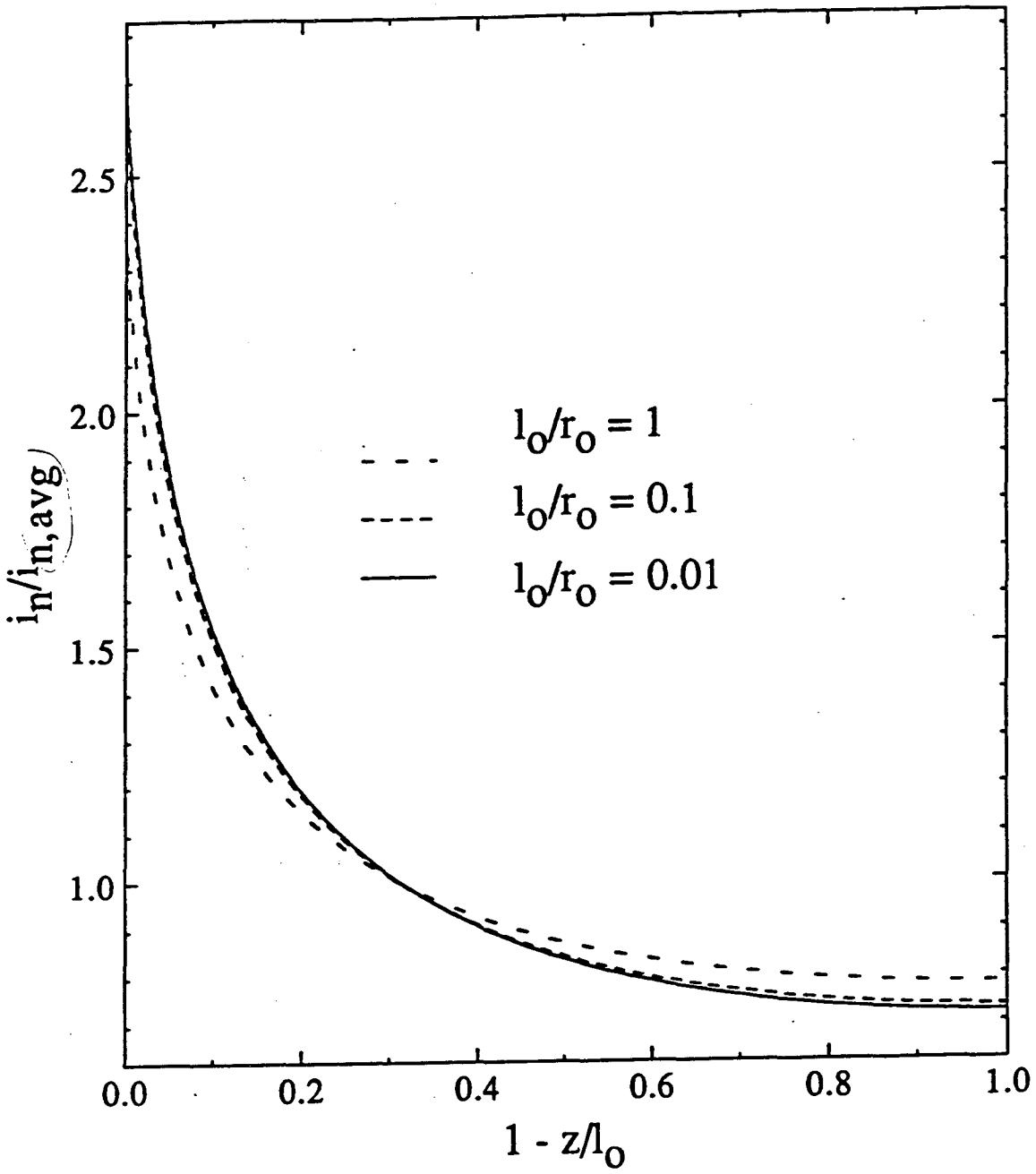

$$\frac{i_{edge}}{i_{center}} = 1 + J_r \frac{\kappa \Delta \Phi_0}{i_c r_0} \quad \text{for} \quad J_r \to 0. \tag{54}$$

The low-aspect-ratio limit on figure 6 gives $1+(2\ln 2)J_l / \pi$ for the right side of this equation. For the current density to vary by less than one percent from the minimum at the center of the electrode to the maximum at the edge, we should require J_l to be less than roughly 0.02, and this is plotted on figure 11. The high-aspect-ratio limit on figure 6 gives $1+0.5 J_r \ln(l_0 / 2\beta r_0)$ for the right side of equation 54. Thus this equation, together with its asymptotic forms, gives the boundary between uniform and nonuniform current distributions on figure 11.

As l_0 / r_0 approaches infinity (the upper left in figure 11), one might suspect that only J_r governs the secondary current distribution in the electrode edge region. However, numerical results show that l_0 / r_0 also influences the current distribution, and indeed such large-aspect-ratio electrodes have both curvature and length. Equation 51 illustrates this point, for large J_r. Figure 3 shows $P_0 / i_{avg}\sqrt{r_0}$ increasing as l_0 / r_0 approaches infinity. Thus, for large J_r, i_{edge} / i_{avg} increases as l_0 / r_0 approaches infinity. The line of demarcation in this region of figure 11 also shows a dependence on l_0 / r_0.

Acknowledgment

This work was supported by the Assistant Secretary for Conservation and Renewable Energy, Office of Transportation Technologies, Electric and Hybrid Propulsion Division of the U. S. Department of Energy under Contract No. DE-AC03-76SF00098.

Nomenclature

a_j current-function coefficient

$B(\zeta)$ ring-source correction coefficient

f_j current function

F dimensionless ring-source correction function

F Faraday's constant, 96,487 C/equiv

G dimensionless ring-source potential

G^*	dimensionless ring-source potential, including F
i	current density, A/cm^2
i_c	constant current density on the electrode surface, A/cm^2
i_{center}	current density at the electrode center, A/cm^2
i_n	current density on the electrode surface, A/cm^2
i_{avg}	average current density on the electrode surface, A/cm^2
i_{edge}	current density at the electrode edge, A/cm^2
i_0	exchange current density, A/cm^2
J_l	polarization parameter containing l_0
J_r	polarization parameter containing r_0
$K(m)$	complete elliptic integral of the second kind
K_0	modified Bessel function of the second kind of order 0
l_0	electrode center-to-edge distance, cm
m	dimensionless elliptic integral variable
P_{2j}	even Legendre Polynomial of order $2j$
P_0	primary-distribution asymptotic edge-region coefficient, A/cm$^{1.5}$
r	radial distance coordinate, cm
r_0	cylinder radius, cm
R	primary resistance, Ω
R	universal gas constant, 8.3143 J/mol-K
R^*	dimensionless radial distance coordinate
T	absolute temperature, K
V	electrode potential, V
x	distance from the electrode edge, cm
z	axial distance coordinate, cm
z'	axial location of ring source, cm
Z	dimensionless axial distance from ring source

α_a, α_c kinetic transfer coefficients for the anodic and cathodic reactions

β dimensionless parameter characterizing ring-source behavior near the ring

ζ separation-of-variables constant

κ conductivity, $S \cdot cm^{-1}$

σ edge region where finite electrode kinetics limit the electrode current density for high polarization parameters, cm

ϕ dimensionless function for secondary current distribution in the edge region for high polarization parameters

Φ electric potential, V

Φ_0 electric potential on the electrode or insulator, V

References

1. J. S. Newman, *Electrochemical Systems*, Prentice-Hall, Englewood Cliffs, N. J. (1991).

2. A. Weisselberg, "Distribution of Current Along a Cylindrical Anode inside of a Concentric Tube with Applications to Chromic Plating," *Trans. Electrochem. Soc.*, **90**, 235 (1946).

3. A. Weisselberg, *ibid.*

4. R. Alkire and R. Varijan, "Resistive Wire Electrodes," *J. Electrochem. Soc.*, **121**, 622 (1974).

5. R. Strommen and A. Rodland, "Corrosion Surveillance of Submarine Pipelines by Electric Field Strength Monitoring," *Materials Performance*, **20** (10), 47 (1981).

6. John Newman, "The Fundamental Principles of Current Distribution and Mass Transport in Electrochemical Cells," Allen J. Bard, ed., *Electroanalytical Chemistry* (New York: Marcel Dekker, Inc., 1973), **6**, 187-352.

7. Milton Abramowitz and Irene A. Stegun, eds., *Handbook of Mathematical Functions* (Washington, D. C.: National Bureau of Standards, 1964), p. 590.

8. C. Y. Mak, "Potential and Current Distributions on a Band Electrode Embedded in an Infinitely Long, Insulating Cylinder," unpublished paper (1981).

9. Anthony Joseph Grabowski, *Current and Potential Distributions on a Cylinder Electrode*, M. S. Thesis, University of California, Berkeley, July, 1990 (LBL-29312).

10. K. Nişancioğlu and J. Newman, "The Short-Time Response of a Disk Electrode," *J. Electrochem. Soc.*, **121**, 523 (1974).

11. William H. Smyrl and John Newman, "Current Distribution at Electrode Edges at High Current Densities," *J. Electrochem. Soc.*, **136**, 132-139 (1989).

12. C. Wagner, "Theoretical Analysis of the Current Density Distribution in Electrolytic Cells," *J. Electrochem. Soc.*, **98**, 116 (1951).

13. W. R. Parrish and John Newman, "Current Distributions on Plane, Parallel Electrodes in Channel Flow," *J. Electrochem. Soc.*, **117**, 43-48 (1970).

LAWRENCE BERKELEY LABORATORY
UNIVERSITY OF CALIFORNIA
TECHNICAL INFORMATION DEPARTMENT
BERKELEY, CALIFORNIA 94720